Crimson Publishers
Wings to the Research

Review Article

Direct Generation and Kinetic Studies of High-Valent Transition Metal-Oxo Derivatives Through Photochemical Approaches

Rui Zhang*

Department of Chemistry, Western Kentucky University, USA

ISSN: 2637-8035

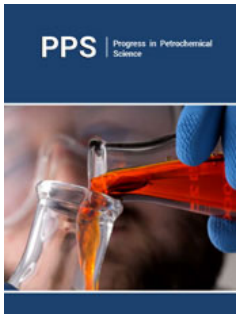

***Corresponding author:** Rui Zhang, Department of Chemistry, Western Kentucky University, USA

Submission: March 18, 2024
Published: March 27, 2024

Volume 6 - Issue 2

How to cite this article: Rui Zhang*. Direct Generation and Kinetic Studies of High-Valent Transition Metal-Oxo Derivatives Through Photochemical Approaches. Progress Petrochem Sci. 6(2). PPS. 000633. 2024.
DOI: 10.31031/PPS.2024.06.000633

Abstract

High-valent transition metal-oxo complexes exhibit a wide range of reactivities and play essential roles as active Oxygen Atom Transfer (OAT) species in many chemical and biological oxidation processes. However, the detection and characterization of these intermediates are still challenging in view of their high reactivity and short lifetimes and their transient nature makes their study complex. This review highlights recent advancements in how photochemical reactions with visible light have emerged as promising approaches to generate and study high-valent transition metal-oxo species with different metals on various macrocyclic ligands. Investigating the reactivity of photo-induced high-valent metal-oxo species through practical kinetic studies has offered valuable insights into the structure-function relationships and an understanding of their involvement in oxidation reactions.

Keywords: Metal-oxo derivatives; Porphyrin; Corrole; Salen; Phthalocyanine, Oxidation; Visible light photolysis; Kinetics

Abbreviations: ESI-MS: Electron Spray Ionization-Mass Spectrometry; ET: Electron Transfer; LFP: Laser Flash Photolysis; OAT: Oxygen Atom Transfer; Por: Porphyrin; Sub-O: Substrate oxidized product; Salen N: N'-bis(salicylidene)ethylenediamine; tBu4-Pc: Tetra-tert-butyl-phthalocyanine; TDCPP: 5,10,15,20-tetra(2,6-dichlorophenyl) porphyrin; TDFPP: 5,10,15,20-tetra(2,6-difluorophenyl) porphyrin; TMP: Tetramesitylporphyrin; TPP: Tetraphenylporphyrin; TPFPP: 5,10,15,20-tetra(pentafluorphenyl) porphyrin; TPC: 5,10,15-triphenylcorrole; TPFC: 5,10,15-tripentafluorophenylcorrole.

Graphic Abstract

Through photo-induced ligand cleavage and photo-disproportionation reactions, diverse high-valent transition metal-oxo derivatives supported by porphyrin, corrole, phthalocyanine and salen ligands have been successfully explored. The reactivity of these metal-oxo species and their catalytic implications are compared and discussed.

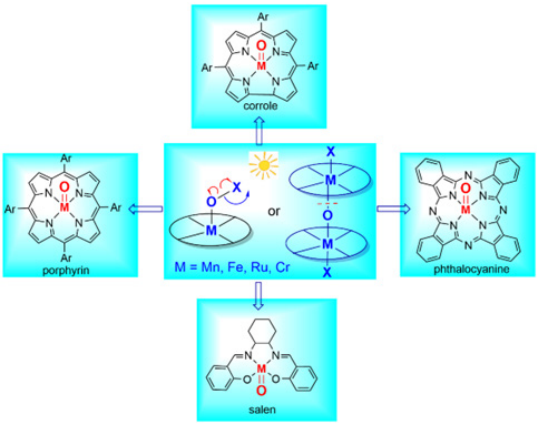

Introduction

High-valent transition metal-oxo species are important Oxygen Atom Transfer (OAT) species that play a significant role in a wide range of oxidation reactions, catalysis and enzymatic processes [1-3]. Remarkably, in nature, the ubiquitous cytochrome P450 enzymes utilize an iron (IV)-oxo radical cation species to activate molecular oxygen, facilitating the oxidation of unreactive C-H bonds with exceptionally high efficiency and selectivity [4-6]. Consequently, the effective production and examination of reactive metal-oxo species have provided valuable insights into the identity of true oxidants and further enhanced our understanding of oxidation mechanisms. This, in turn, advances the development of enzyme-like catalysts for practical applications. However, the characterization of high-valent metal-oxo species is often challenging due to their transient nature and low concentration [7,8]. In biomimetic model studies, these oxo species are typically produced by the reaction of a metal complex with a suitable terminal oxidant, such as hydrogen peroxide, peroxyl acids or a hypervalent iodine reagent [9,10]. In some cases, spectroscopic observation of these intermediates is possible by rapid mixing techniques at low temperatures or by generating relatively stable analogs [11-15]; but in many cases, the actual metal-oxo species responsible for oxidation is not formed at detectable amounts and therefore, remains the subject of speculation. Indeed, the lack of kinetic and mechanistic information often complicates the understanding of the nature of the active oxidants in homogeneous catalysis.

Our research group has engaged in a general study to probe oxidation catalysis that aims at photochemical generation and direct examination of reactive high-valent transition metal-oxo intermediates involved in the respective oxidation processes [16,17]. Photochemistry offers a promising alternative for producing highly reactive metal-oxo transients with some advantages [18,19]. Unlike conventional chemical methods that use toxic or polluting reagents, photochemical reactions involve the absorption of a photon for activation without leaving any residue. More importantly, photochemical approaches offer much higher temporal resolution than the fastest mixing studies, which is essential for detecting highly reactive transients [16]. For example, Laser Flash Photolysis (LFP) techniques have been successfully employed to produce a range of transient metal-oxo species on a timescale as short as a sub-microsecond [20-24]. In this mini review, we describe our progress in developing two distinct photochemical approaches to probe high-valent transition metal-oxo derivatives supported by various macrocycles. Meanwhile, we demonstrate that direct kinetic studies in real time can offer mechanistic insights into the reactivities and identities of the active oxidants in the catalytic processes.

The first approach involves photo-induced ligand cleavage reactions, in which we photolyze metal complexes in the n oxidation state with oxygen-containing ligands such as chlorate, bromate or nitrite. Homolysis of the O-X bond in the ligand results in metal-oxo species in (n+1) oxidation state, while heterolysis gives (n+2) oxidation state metal-oxo species (Figure 1A). The specific reaction pathways depend on many factors, such as the photo-labile precursors, transition metals and their initial oxidation states and the macrocyclic ligands. The second approach employs photo-disproportionation reactions [25-27] in which photolysis of a μ-oxo dimeric M^n complex produces an M^{n+1}-oxo species and an M^{n-1} reduced product (Figure 1B). In the presence of large concentrations of reductants, single turnover reactions with respect to the metal-oxo oxidant can be achieved, enabling easy kinetic measurements of second-order rate constants under pseudo-first-order conditions. Although the concept of photo protocols for producing metal-oxo species is straightforward, successful creation requires considerable development of the requisite photochemical reactions and especially the photo-labile precursors.

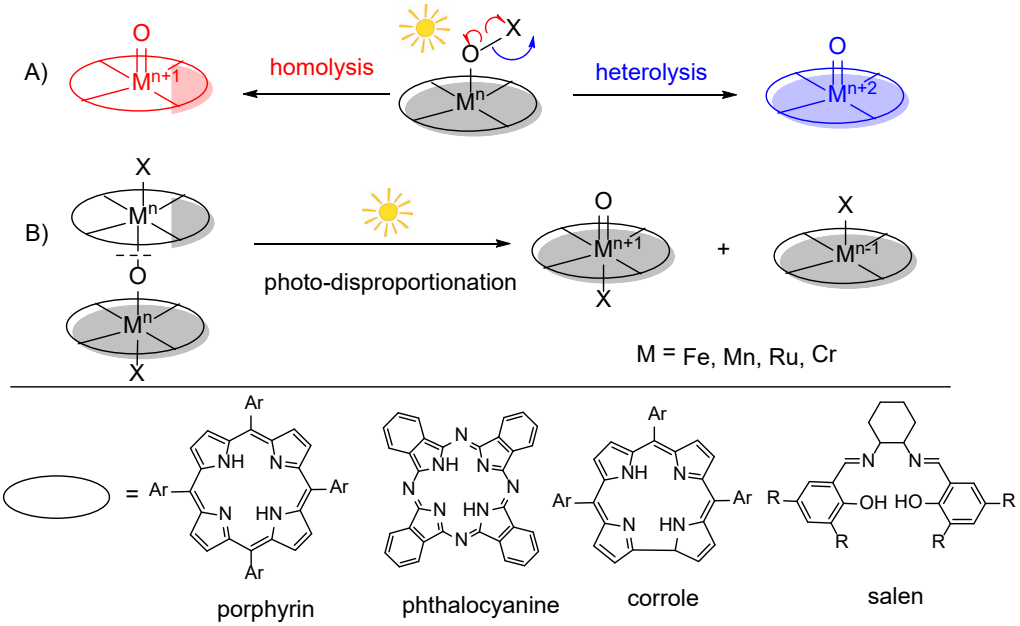

Figure 1: Production of high-valent metal-oxo intermediates through (A) visible light-induced ligand cleavages, and (B) photo-disproportionation reactions.

High-Valent Manganese-Oxo Species

Manganese (IV)-oxo porphyrins [Mn^{IV} (Por)(O)]

High-valent manganese-oxo species are known for their reactivity in oxidation catalysis and have been extensively examined as bioinspired synthetic catalysts [12,28]. In this context, highly reactive porphyrin-manganese(V)-oxo derivatives have been implicated as the primary oxidants [29,30] and their detection has been achieved by chemical or LFP methods [31-33]. Additionally, trans-dioxo manganese(V) porphyrins were chemically synthesized and exhibited pH-dependent reactivities towards typical substrates [34]. However, manganese (IV)-oxo porphyrins have received less attention primarily due to their relatively low reactivity [35-38]. To address this, we have explored two photochemical methods using visible light to produce and study a series of porphyrin-manganese (IV)-oxo species.

Visible light photolysis of the highly photo-labile porphyrin-Mn^{III} chlorate or bromate salts (1) effectively produced three [Mn^{IV} (Por)(O)] (2a-c) with varying electronic structures (Figure 2, path a) [39]. The systems under study include [Mn^{IV} (TPFPP)(O)] (2a), [Mn^{IV} (TDFPP)(O)] (2b) and [MnIV (TMP)(O)] (2c). The photo-generation of 2 was rationalized by homolysis of the O-X (X = Cl or Br) bonds in the ligands, resulting in one-electron oxidation on the metal that is consistent with findings from previous LFP studies [33]. The identification of photo-generated porphyrin-manganese (IV)-oxo species was substantiated through ESI-MS analysis and further validated by synthesizing the same species via chemical oxidation of the corresponding manganese (III) chloride using PhI $(OAc)_2$ [39]. Alternatively, visible light irradiation of manganese (III)-μ-oxo bis-porphyrins (3d-f) in three sterically unencumbered porphyrin systems resulted in photo-disproportionation reactions that directly led to the formation of manganese (IV)-oxo porphyrins along with manganese (II) products (not shown here) in benzene solutions (Figure 2, path b) [40]. Attempts to synthesize the μ-oxo dimers with sterically hindered porphyrins (3a-c) were unsuccessful. In the absence of substrate, the initially formed manganese (II) species was highly transient and underwent rapid aerobic oxidation to give manganese (III) porphyrins. Continuous irradiation of dimanganese (III) μ-oxo bis-porphyrins in the presence of strong donors such as Pyridine (Py) or Triphenylphosphine (Ph_3P) gave rise to the formation of stable [Mn^{II} (Por)(Py)] or [Mn^{II} (Por)(PPh_3)]. This observation provides additional support for the photo-disproportionation mechanism previously established for diiron (III) μ-oxo bis-porphyrins [41].

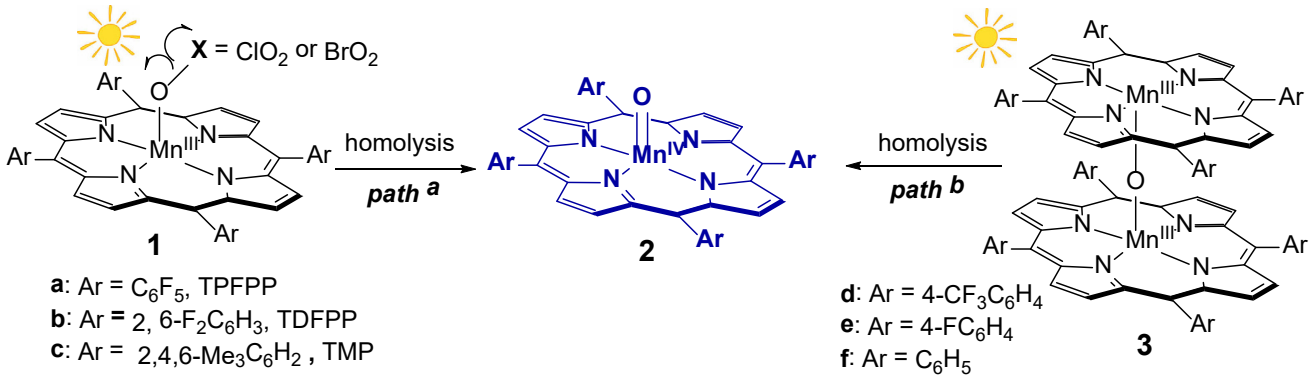

Figure 2: Two photochemical entries to Mn^{IV}-oxo porphyrins.

Manganese(V)-oxo corroles [Mn^{V} (Cor)(O)]

Tri-anionic corroles are contracted analogues of porphyrins and able to stabilize higher metal oxidation states. Consequently, relatively stable manganese (V)-oxo corroles, denoted as [Mn^{V} (Cor)(O)], have been reported as active OAT species [42]. However, the mechanism of the reactions involving [Mn^{V} (Cor)(O)] are intricate [43,44] and the factors governing their OAT reactivity with organic substrates are not yet fully understood. As outlined in Figure 3, photo-induced ligand cleavage reactions were utilized to produce corrole-manganese(V)-oxo species cross three distinct ligand systems [45,46]. To accomplish this, one-electron oxidations of corrole-manganese (III) salts afforded corrole-manganese (IV) chlorides [42] that underwent facile ligand exchange with $AgXO_3$ (X = Cl and Br) or $AgNO_2$ to generate the corresponding photo-labile precursors (4). As anticipated, visible light irradiation of 4 led to homolytic cleavage of the ligand O-Cl bond to give corrole-manganese(V)-oxo species (5), showing the same UV–visible spectra as those formed by chemical oxidations with ozone or iodosylbenzne (PhIO) [42,47].

The reactivity and reaction pathways of [Mn^{V} (Cor)(O)] are markedly influenced by solvent and ligand effects [45]. In the polar solvent CH_3CN, the electron-deficient system [Mn^{V} (TPFC)(O)] (5a) reverted to MnIII corrole at the end of the oxidation reactions. Conversely, in the less polar solvent CH_2Cl_2 or in non-electron-deficient systems (5b and 5c), the Mn^{IV} product was formed instead. Moreover, the reactivity order of [Mn^{V} (Cor)O] with the same substrates and solvent was found to be 5c > 5b > 5a, contrary to expectations based on the electron-demand of the corrole ligands. The spectral and kinetic patterns align with multiple oxidation pathways, wherein 5 acts as either a direct two-electron oxidant or undergoes a disproportionation reaction to form a manganese (VI)-oxo corrole as the primary oxidant [45].

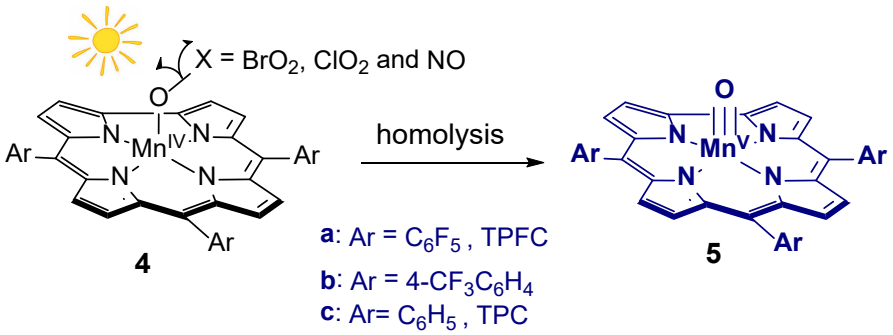

Figure 3: Photo-generation of manganese(V)-oxo corroles.

Manganese (IV)-oxo phthalocyanine [Mn^{IV} (Pc)(O)]

Metal Phthalocyanine Complexes (MPc's) have gained a significant interest as bioinspired catalysts due to their structural similarity to heme-containing macrocycles and exceptional redox and optical properties [48-51]. However, their mechanistic understanding lags behind that of their metalloporphyrin counterparts, mainly due to the lack of Pc-metal-oxo intermediates and limited knowledge of their reactivities. Very recently, we made an important advance by expanding the analogous photo-ligand cleavage reactions to generate and examine a novel manganese (IV)-oxo phthalocyanine species (6) (Figure 4) [52]. Prior to this work, only one high-valent iron (IV)-oxo radical cation species on the phthalocyanine platforms was detected and spectroscopically characterized [53].

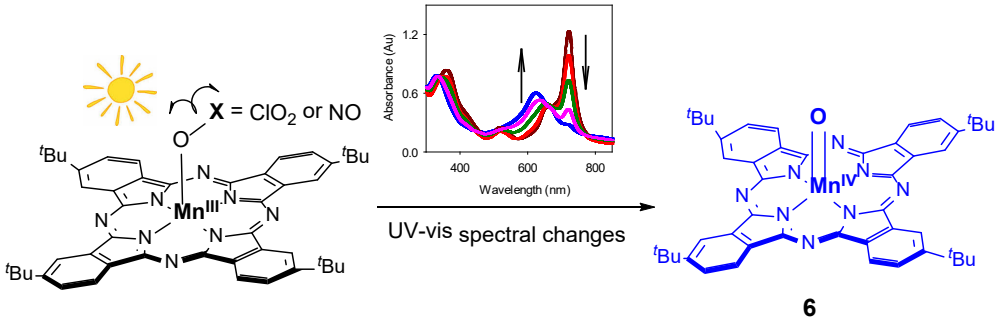

Figure 4: Photo-generation of a new manganese (IV)-oxo phthalocyanine monitored by UV-vis spectroscopy.

The photo-generated species 6, i.e. [Mn^{IV}(tBu4-Pc) (O)], was characterized by Electron Spray Ionization Mass Spectrometry (ESI-MS), revealing an expected molecular ion at m/z =808 along with exchange of the oxo ligand with isotope-labelled $H_2{}^{18}O$. This observation aligns with the anticipated characteristic of high-valent metal-oxo species. Following its generation, the reactivity of the newly formed manganese (IV)-oxo species was kinetically explored using various organic substrates such as alkenes, benzylic hydrocarbons, alcohols and sulfides. The second-order rate constants (k_{ox}) range from 4.1 × 10^{-3} $M^{-1}s^{-1}$ for cis-cyclooctene to 1.3 $M^{-1}s^{-1}$ for thioanisole, which are comparable to the known manganese (IV)-oxo porphyrins (2) [39]. This study marks the first photochemical generation and reactivity study of metal-oxo species on the phthalocyanine platform that can be directly compared with the related porphyrin-metal-oxo species.

High-Valent Iron-Oxo Porphyrins

Among high-valent metal-oxo species, reactive iron-oxo porphyrins have particularly attracted attention due to their importance in various oxidative enzymes found in nature and their unique properties for broad applications [54,55]. The readily accessible high oxidation state of iron is +4 and heme and non-heme iron (IV)-oxo species are well-known and documented [3]. Catalytic cycles in heme-containing peroxidase, catalase, and cytochrome P450 enzymes [56] as well as in synthetic models [11] are often mediated by iron (IV)-oxo porphyrin radical cations, also termed compound I. An exploration of the photo-induced ligand reaction extended to produce iron (IV)-oxo radical cation species (compound I derivatives) or iron (IV)-oxo porphyrin (compound II derivatives), depending on electronic and steric factors within the porphyrin ligands [57,58]. For instance, visible light photolysis of porphyrin-iron (III) bromates or chlorates (7) in electron-rich systems resulted in porphyrin-iron (IV)-oxo radical cations (9a-d). In contrast, photolysis of complexes 7 with electron-deficient and sterically encumbered ligands produced neutral iron (IV)-oxo porphyrins (10e-g).

The profound ligand-dependent formation of iron (IV)-oxo species 9 or 10 can be rationalized by a photo-induced heterolysis of the O-X bond of 7, generating a putative porphyrin-iron(V)-

oxo species (8) (Figure 5). In non-electron-deficient porphyrin systems (a-d), the high-energy iron(V)-oxo species (8) could undergo relaxation to compound I models (9a-d) through internal Electron Transfer (ET) from the porphyrin to the iron, as it is thermodynamically favored (path a). However, the ET process from highly electron-demanding porphyrin systems (e-f) to the iron is apparently unfavorable due to a high redox potential. Instead, a rapid comproportionating reaction of 8 with the remaining iron (III) complex (path b) could produce iron (IV)-oxo derivatives (10e-g). Earlier studies on manganese-oxo species indicated that porphyrin-manganese (V)-oxo species rapidly comproportionate with manganese (III) species, and corrole-manganese (V)-oxo species react with manganese (III) species to produce manganese (IV)-oxo species. The choice between these two possibilities is influenced by the electronic structure and/or redox potential of the porphyrin ligand. This, in turn, determines the electron spin distribution of atomic orbitals and the bond reorganizations required to form the two species.

As expected, the more oxidized compound I derivatives 9 reacted 2-3 orders of magnitude faster than the compound II 10 with the same substrate. Interestingly, the reactivity order for species 10 is inverted with the expectation on the basis of the electron-withdrawing of the porphyrin macrocycles, suggesting that compound II derivatives (10) could undergo a disproportionation reaction to generate a more reactive iron (IV)-oxo porphyrin radical cation (9) as the primary oxidant. Indeed, the direct spectroscopic observation of disproportionation of 10 to 9 under acidic conditions was previously reported [59].

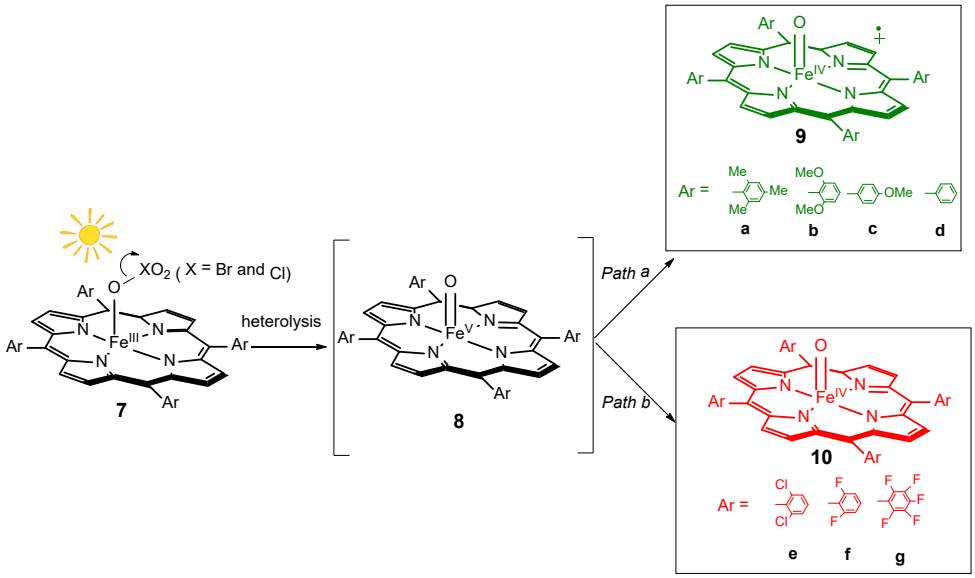

Figure 5: Ligand-dependent photo-generation of porphyrin-iron (IV)-oxo compound I derivatives via ET (Path a) and compound II species via comproportionating pathway (Path b).

High-Valent Ruthenium-Oxo Species

Ruthenium (V)-oxo porphyrins [Ru^{V} (Por)(O)]

Porphyrin-ruthenium (V)-oxo complexes are significant as highly reactive oxidizing intermediates involved in efficient oxidation processes [60-62]. Computational studies suggested that they are thermodynamically more favorable than ruthenium (IV)-oxo porphyrin radical cations [63]. Recently, spectroscopic evidence along with kinetic and computational studies have been reported to support the formation of the highly reactive ruthenium(V)-oxo species as the active oxidant in the ruthenium (III) porphyrin-catalyzed oxidations [64]. In this regard, two distinct photochemical approaches were employed to generate the porphyrin-ruthenium (V)-oxo species (Figure 6). The first involves the photo-disproportionation of a bis-porphyrin-diruthenium (IV) μ-oxo dimer (11) that provides access to the reactive porphyrin-ruthenium (V)-oxo intermediate (12) [27]. The second involves the photo-cleavage of a ruthenium (III) N-oxide adduct (13) to afford the same oxo transient 12 as a result of heterolytic cleavage of the Ru-O bond (Figure 6) [65]. The UV–vis spectra and kinetic behaviors of transients generated from the two routes are indistinguishable.

The oxo species 12 showed remarkable reactivity with representative second-order rate constants of k_{ox} = 6.6 × 10^3 M^{-1} s^{-1} for diphenylmethanol, k_{ox} = 1.8 × 10^3 M^{-1} s^{-1} for cyclohexene and k_{ox} = 1.3 × 10^3 M^{-1} s^{-1} for cis-cyclooctene. Notably, the potential use of photo-disproportionation reactions for photocatalytic aerobic oxidations is particularly appealing [26]. Accordingly, the successful realization of the proposed photocatalytic cycle relies on the crucial regeneration of the μ-oxo dimers through aerobic oxidation of the resulting ruthenium (III) intermediate [66]. In this regard, a series of diruthenium (IV) μ-oxo bis-porphyrins [27] have demonstrated their ability to catalyze the demanding aerobic oxidation of hydrocarbons through a photo-disproportionation mechanism, similar to that of well-known diiron (III)-μ -oxo bis-porphyrin complexes [41]. The catalytic sequence is sustainable because it uses visible light to activate molecular oxygen for organic oxidations without the need for external co-reductants [67].

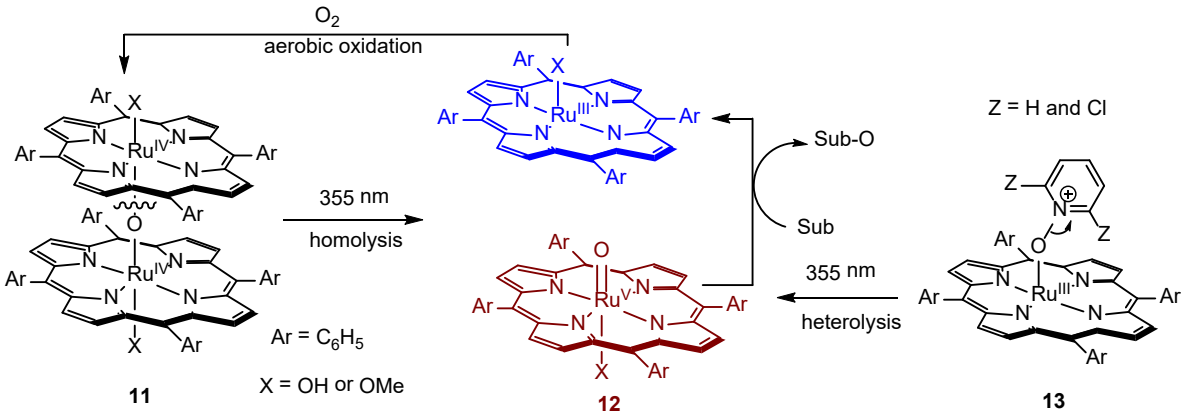

Figure 6: Two photochemical entries to highly reactive Ru^{V}-oxo porphyrins.

Trans-dioxoruthenium (VI) porphyrins [Ru^{VI} (Por)$(O)_2$]

Trans-Dioxoruthenium (VI) porphyrins are structurally well-defined model systems for heme-containing enzymes [68,69], but they are much less reactive compared to ruthenium (V)-oxo counterparts [70]. As for photochemical generation, the photo-labile precursors dihalorate [Ru^{IV} (Por)$(XO_3)_2$] (14, X = Cl or Br) were obtained by facile exchange of the counterions in literature-known [Ru^{IV} (Por)Cl_2] [71] with $AgXO_3$. Similarly to previously mentioned for manganese (IV)-oxo and iron (IV)-oxo species, the visible light photolysis of [Ru^{IV} (Por)$(XO_3)_2$] proceeded simultaneous homolytic cleavage of two X-O bonds (double homolysis), which resulted in the formation of trans-dioxo species (15) within diverse electronic and steric porphyrin systems (Figure 7). This photo protocol demonstrated a broader generality compared to chemical methods [72,73]. Under identical conditions, it was observed that the bromate precursors exhibited greater photo efficiency compare to the chlorates. The OAT reactions from 15 to organic sulfides were kinetically investigated with tunable structural and electronic properties [74]. The sulfoxidation reactions of dioxoruthenium (VI) species 14 demonstrated impressive reactivity with second-order rate constants ranging from 8 to 60 M^{-1} s^{-1}, which are 3 orders of magnitude larger than those of well-studied alkene epoxidations and activated C-H bond oxidations [74]. In addition, the reactivity order for 14 correlated well with the expectation based on the electron-withdrawing and steric effects of the porphyrin macrocycles.

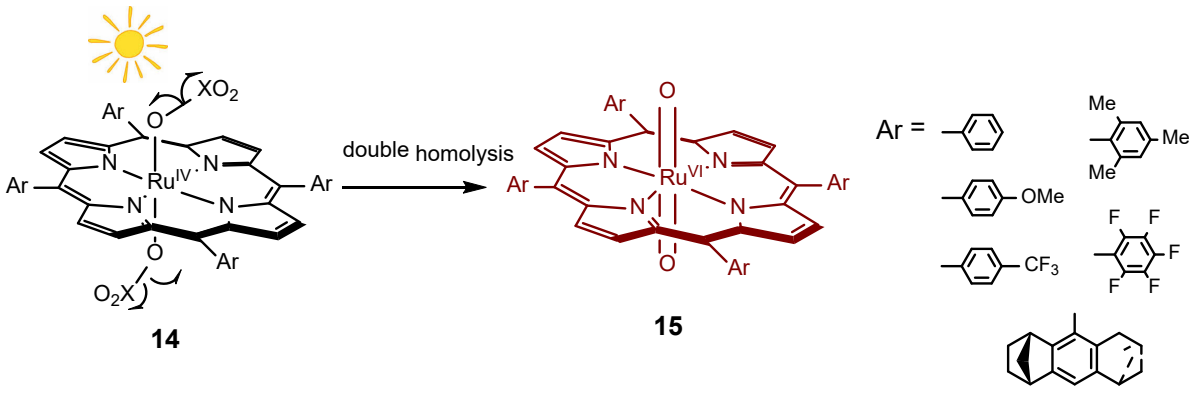

Figure 7: Photosynthesis of *trans*-dioxoruthenium (VI) porphyrins.

High-Valent Chromium-Oxo Species

Chromium (V)-oxo [Cr^{V} (Por)(O)] and chromium (IV)-oxo porphyrins [Cr^{IV} (Por)(O)]

The intricate chemistry of high-valent chromium-oxo porphyrins or salens have taken center stage as biomimetic models because of their easy accessibility and stability [75]. In chromium porphyrin systems, two distinct high-valent species, chromium(V)-oxo and chromium (IV)-oxo porphyrins, are well known [76,77]. We explored the photo-generation and kinetics of these species in three systems for sulfoxidation reactions [78]. In addition to the chemical oxidation of chromium (III) complexes by PhI $(OAc)_2$, the visible-light irradiation of chromium (III) chlorates provides alternative access to [Cr^{IV} (Por)(O)] (16). One-electron oxidation [79] of the resulting species 16 with $AgClO_4$ produced chromium(V)-oxo species, i.e. [Cr^{V} (Por)(O)]$^{+}$ (17) in CH3CN solution (Figure 8). Both the chromium (IV)- and chromium(V)-oxo species exhibited sufficient stability for characterization by ESI-MS, displaying distinct peaks at the expected M+1 ions, respectively. Additionally, the ESI-MS measurement of chromium(V)-oxo species disclosed an isotope exchange in the oxo ligand with $H_2{}^{18}O$. As anticipated, the diamagnetic nature of [Cr^{IV} (TMP)(O)] was confirmed by well-resolved 1H NMR spectroscopy.

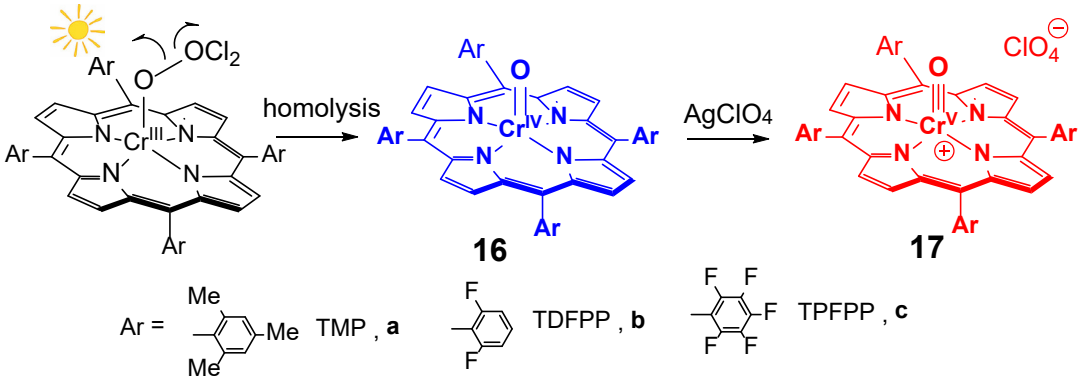

Figure 8: Generation of chromium (IV)/(V)-oxo porphyrins.

Comprehensive kinetic studies enable a direct comparison of the reactivities of porphyrin-chromium (IV)/(V)-oxo complexes in sulfoxidation reactions under identical conditions. Consistent with expectation, chromium(V)-oxo species 17 are several orders of magnitude more reactive than the respective 16. Among chromium(V)-oxo species, substantially greater rate constants were obtained with electron-deficient [Cr^{V} (TDFPP)(O)]+ (17b) and [Cr^{V} (TDFPP)(O)]$^{+}$ (17c) systems compared to the electron-rich [Cr^{V} (TDFPP)(O)]$^{+}$ (17a). Hammett analyses indicate significant charge transfer in the transition states for oxidation of para-substituted thioanisoles by 17, suggesting a mechanism that involves the electrophilic attack of the CrV-oxo at sulfides to form a sulfur cation intermediate in the rate-determining step [42].

Chromium (V)-oxo salens [Cr^{V} (salen)(O)]

Metallosalens contain a cramp-like tetradentate motif and share catalytic features in common with metalloporphyrin's [80]. Due to their high stability, chromium (V)-oxo salens are well known in literature and have been fully characterized by various spectroscopic methods [81]. Recent progress was reported on the visible light generation of chromium (V)-oxo complexes i.e., [Cr^{V} (salen)O] (18) bearing the well-known Jacobsen salen ligand and its derivative (Figure 9) [82]. This marks the first instance where photochemical production of metal-oxo species extends beyond porphyrinoid ligands, demonstrating feasibility of photochemical approaches with simple, easily constructed salen-based complexes. The photo-generated 18 exhibited a well-known characteristic absorption feature and was further characterized by ESI-MS. Of note, 18 is spectroscopically and kinetically indistinguishable from that formed by the reported chemical oxidation [81]. Additionally, our unpublished results also indicated that photolysis of [Mn^{III} (salen)(XO_3)] resulted in the formation of OAT species that were tentatively assigned as cationic [Mn^{V}(salen)O]$^{+}$ in view of their absorption spectra and reactivity behaviors. Kinetic studies revealed that the reactivity of [Mn^{V}(salen)O]$^{+}$ is one order of magnitude greater than that of 18 supported by the same salen ligand.

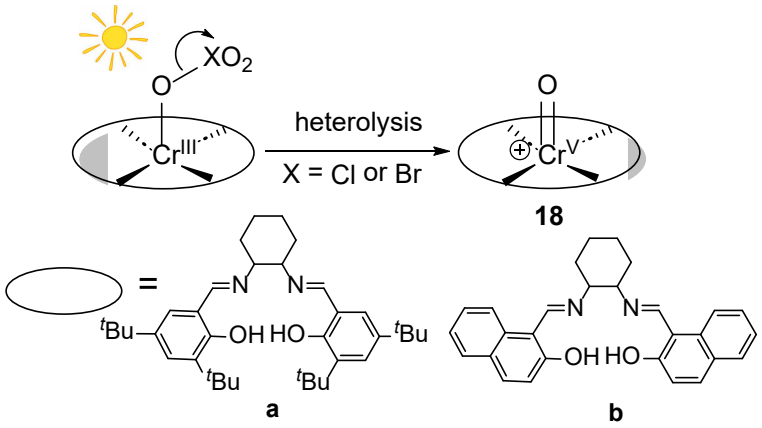

Figure 9: Photo-generation of chromium (V)-oxo salens.

Reactivities of Metal-Oxo Species and Implications for Catalytic Oxidations

The photochemical generation of high-valent metal-oxo species permits kinetic studies in a wide variety of oxidation reactions, allowing for a direct comparison of their reactivities under analogous conditions. Table 1 contains some representative rate constants of various metal-oxo species supported by different macrocyclic ligands, including porphyrins, phthalocyanines, corroles or salen. Table 1 also includes the rate constants of manganese(V)-oxo porphyrin cation that were obtained from previous LFP kinetic studies [33]. Upon reviewing Table 1, it becomes apparent that the reactivity of metal-oxo species is predominantly dictated by the metal center and its oxidation states. For example, porphyrin manganese(V)-oxo derivatives have the same formal oxidation state as the iron (IV)-oxo porphyrin radical cations, but they

react 5 orders of magnitude faster than the latter with the same substrate. Additionally, the porphyrin ruthenium(V)-oxo species exhibits 3 to 5 orders of magnitude higher reactivity than the porphyrin chromium(V)-oxo and salen chromium(V)-oxo species. In general, higher oxidation states lead to greater reactivities with manganese(V)/chromium(V)-oxo porphyrins being several orders of magnitude more reactive than the corresponding meta l(IV)-oxo counterparts with the same TPFPP ligand. Moreover, the nature of the ligand coordinated with the metal center plays a significant role in the reactivity due to the modification of the electronic and steric properties of the metal-oxo species. For example, the corrole ligands are trianionic, as opposed to dianionic porphyrin ligands, and thereby corrole-manganese(V)-oxo species are inherently more stable than the porphyrin-manganese(V)-oxo analogs. Lastly, the nature of the substrate also impacts the reactivity as different substrates possess varying nucleophilicities, steric hindrance, and availability to the metal-oxo moiety, resulting in different oxidation rates and/or OAT mechanisms.

Table 1: Second-order rate constants of various metal-oxo species under similar conditions.

Metal-oxo species	Cis-cyclooctene	Ethylbenzene	Thioanisole
$[Mn^{IV}$ (TPFPP)(O)] (2a)	1.5×10^{-1}	7.1×10^{-1}	1.7
$[Mn^{IV}$ (tBu4-Pc) (O)] (6)	4.1×10^{-3}	1.8×10^{-2}	1.3
$[Fe^{IV}$ (TPFPP)(O)] (10g)	1.8×10^{-2}	4.6×10^{-2}	46
$[Cr^{IV}$ (TPFPP)(O)] (16c)	n.d.[b]	n.d.[b]	1.4
$[Fe^{IV}$ (TMP)(O)]$^{+}$·(9a)	1.2×10^{2}	6.2	
$[Mn^{V}$ (TPFPP)(O)]$^{+}$[c]	6.1×10^{5}	1.1×10^{5}	
$[Mn^{V}$ (TPFC)(O)] (5a)	2.9×10^{-3}	1.4×10^{-4}	4.9
$[Ru^{V}$ (TPP)(O)]$^{+}$ (12)	1.3×10^{3}		
$[Cr^{V}$ (TPFPP)(O)]$^{+}$ (17c)	8		2.2×10^{3}
$[Cr^{V}$ (salen(O)]$^{+}$ (18)	3.0×10^{-2}		5.8×10^{-2}

(a)Second-order rate constants in units of M^{-1} s^{-1} for reactions in CH_3CN at 23 ± 2 °C. (b) n. d. = not detected due to no decay of species 16 in the presence of excess substrates. (c) from Ref. 33.

Meanwhile, available kinetic results from this study offer profound insights into the identification of the actual OAT oxidants in catalytic turnover conditions with transition metal catalysts, where the concentrations of active oxidants, in most cases, do not accumulate to detectable levels. By identifying the kinetically competent oxidants, we could improve control over the catalytic oxidation reactions, especially in terms of selectivity. To assess whether the observed metal oxo species in our direct kinetic studies are active oxidants under catalytic turnover conditions, one approach is to compare the ratios of products formed under catalytic turnover conditions to the ratios of rate constants measured in the direct kinetic studies [16]. If the same oxidant is present in both cases, the ratios of absolute rate constants from direct measurements and relative rate constants from the competition studies should be similar. When the ratios are not similar, however, the active oxidants under the two sets of conditions must be different. For example, competition studies with chromium (III) porphyrin chloride and PhI $(OAc)_2$ gave relative rate constants for oxidations of competing thioanisoles that closely match ratios of absolute rate constants from chromium(V)-oxo species (16), suggesting it serves as true oxidants under catalytic conditions [78]. However, our mechanistic studies of porphyrin-manganese (IV)-oxo 2, [39] corrole-manganese (V)-oxo 5, [20a] and porphyrin-iron (IV)-oxo 10 [83] indicate that a high-valent metal-oxo species detected in a reaction might not be the true or sole oxidant in these systems.

Summary and Outlook

This mini review offers an overview of our recent advancements in the photo-induced formation of diverse high-valent metal-oxo species, as published to date. Generation of high-valent transition metal-oxo derivatives through photochemical approaches holds great promise for general synthetic utility, encompassing a variety of known and unknown metal-oxo species featuring different metals supported by porphyrin, corrole, phthalocyanine and salen ligands. The photochemical approaches using visible light are simple, green and appealing alternatives as a strategic departure from conventional methods. In particular, the kinetics of oxidation reactions with the photo-generated metal-oxo species can be readily measured under pseudo-first-order conditions at ambient temperatures without convolution from the excess oxidants typically associated with chemical methods. This approach opens avenues for directly comparing reactivities of various metal-oxo species and provides valuable insights into understanding the true oxidants involved in the catalytic oxidation reactions.

In future research, photo-synthetic methodologies will continue to be explored to produce other high-valent metal-oxo intermediates, especially those yet undiscovered. Despite the advancements made in the current photochemical strategies, several challenges remain to be addressed. Spectroscopic characterization of these metal-oxo transients proves challenging due to their low concentration and high reactivity. It should be noted that producing metal oxo in most cases was limited to low concentrations, typically ranging from 10^{-5} to 10^{-6}M. This is because higher concentrations resulted in inert photochemical reactions due to the apparent blockage of the light transmission. Thus, current assignments of photo-generated metal-oxo species are based on limited spectroscopic data obtained thus far. Therefore, more in-depth spectroscopic

characterizations of these novel metal-oxo transients and related species will be essential to provide crucial structural information. To overcome this challenge, emerging photochemical methods will be coupled with advanced technology, such as stopped-flow spectrometers and batch methods at low temperatures, which may be a direction of future works as they offer high temporal resolution and high yield formation for in-depth characterization and studies. As the demand for green and sustainable chemistry grows, the use of visible light (sunlight) rather than a chemical reagent with a photocatalyst offers an attractive means to harness solar energy in applied synthesis [84-86]. A particular emphasis will also be placed on the μ-oxo metal (IV) dimeric complexes as promising photocatalysts that undergo a photo-disproportionation sequence to generate a catalytically reactive metal (V)-oxo species for aerobic photo-oxidations [26,27,87]. The primary objective is to enhance quantum yields and ultimately maximize the efficiency of the photocatalytic process. To this end, we have recently augmented the light-harvesting capabilities of porphyrin by incorporating additional BODIP dye units, resulting in a significant enhancement of the efficiency for photocatalytic oxidation reactions [88].

Acknowledgment

This research has been supported by grants from the National Science Foundation (CHE-2154579). The author thanks the past students and collaborators whose names appear in the list of references. The author also appreciates the financial support of internal grants (RCAP and FUSE) from Western Kentucky University.

References

1. Meunier B (2000) Metal-oxo and Metal-peroxo species in catalytic oxidations. (1st edn), Springer Berlin, Heidelberg, pp. X-323.
2. Groves JT, Shalyaev K, Lee J (2000) The porhyrin handbook. In: Kadish KM, Smith KM, Guilard R (Eds.), Academic Press, pp. 17-40.
3. Costas M, Mehn MP, Jensen MP, Que L (2004) Dioxygen activation at mononuclear nonheme iron active sites: Enzymes, models and intermediates Chem Rev 104(2): 939-986.
4. Montellano PR (2005) Cytochrome P450 structure, mechanism and biochemistry. (3rd edn), Kluwer Academic/Plenum, New York, USA.
5. Denisov IG, Makris TM, Sligar SG, Schlichting I (2005) Structure and chemistry of cytochrome P450. Chem Rev 105(6): 2253-2277.
6. Huang X, Groves JT (2018) Oxygen activation and radical transformations in heme proteins and metalloporphyrins. Chem Rev 118(5): 2491-2553.
7. Rittle J, Green MT (2010) Cytochrome P450 compound I: Capture, characterization and C-H bond activation kinetics. Science 330(6006): 933-937.
8. Wang X, Peter S, Kinne M, Hofrichter M, Groves JT (2012) Detection and kinetic characterization of a highly reactive heme-thiolate peroxygenase compound I. J Am Chem Soc 134(31): 12897-12900.
9. Meunier B (1992) Metalloporphyrins as versatile catalysts for oxidation reactions and oxidative DNA cleavage. Chem Rev 92(6): 1411-1456.
10. Che CM, Huang JS (2009) Metalloporphyrin-based oxidation systems: From biomimetic reactions to application in organic synthesis. Chem Commun (27): 3996-4015.
11. Watanabe Y, Fujii H (2000) Metal-oxo and metal-peroxo species in catalytic oxidations. In: Meunier B (Eds.), Springer-Verlag, Berlin, pp. 61-89.
12. Baglia RA, Zaragoza JP, Goldberg DP (2017) Biomimetic reactivity of oxygen-derived manganese and iron porphyrinoid complexes. Chem Rev 117(21): 13320-13352.
13. McGown AJ, Badiei YM, Leeladee P, Prokop KA, Debeer S, et al. (2011) Handbook of porphyrin science. In: Kadish KM, Smith KM, Guilard R, World Scientific Press.
14. Aviv I, Gross Z (2007) Corrole-based applications. Chem Commun (20): 1987-1999.
15. Neu HM, Baglia RA, Goldberg DP (2015) A balancing act: Stability versus reactivity of Mn(O) complexes. Acc Chem Res 48(10): 2754-2764.
16. Zhang R, Newcomb M (2008) Laser flash photolysis generation of high-valent transition metal-oxo species: Insights from kinetic studies in real time. Acc Chem Res 41(3): 468-477.
17. Zhang R, Klaine S, Alcantar C, Bratcher F (2020) Visible light generation of high-valent metal-oxo intermediates and mechanistic insights into catalytic oxidations. J Inorg Biochem 212: 111246.
18. Yoon TP, Ischay MA, Du J (2010) Visible light photocatalysis as a greener approach to photochemical synthesis. Nature Chem 2(7): 527-532.
19. Ener ME, Lee YT, Winkler JA, Gray HB, Cheruzel L (2010) Photooxidation of cytochrome P450-BM3. Proc Natl Acad Sci U S A 107(44): 18783-18786.
20. Zhang R, Newcomb M (2003) Laser flash photolysis formation and direct kinetic studies of manganese(V)-oxo porphyrin intermediates. J Am Chem Soc 125(41): 12418-12419.
21. Harischandra DN, Zhang R, Newcomb M (2005) Photochemical generation of a highly reactive iron-oxo intermediate. A true iron(V)-oxo species? J Am Chem Soc 127(40): 13776-13777.
22. Newcomb M, Zhang R, Chandrasena RE, Halgrimson JA, Horner JH, et al. (2006) Cytochrome P450 compound I. J Am Chem Soc 128(14): 4580-4581.
23. Pan Z, Zhang R, Fung LW, Newcomb M (2007) Photochemical production of a highly reactive porphyrin-iron-oxo species. Inorg Chem 46(5): 1517-1519.
24. Pan Z, Wang Q, Sheng X, Horner JH, Newcomb M (2009) Highly reactive porphyrin-iron-oxo derivatives produced by photolyses of metastable porphyrin-iron (IV) diperchlorates. J Am Chem Soc 131(7): 2621-2628.
25. Richman RM, Peterson M (1982) Photodisproportionation of .mu. -oxo-bis[(tetraphenylporphinato)iron (III)]. J Am Chem Soc 104(21): 5795-5796.
26. Harischandra DN, Lowery G, Zhang R, Newcomb M (2009) Production of a putative iron (V)-oxocorrole species by photo-disproportionation of a bis-corrole-diiron (IV)-μ-oxo dimer: Implication for a green oxidation catalyst. Org Lett 11(10): 2089-2092.
27. Vanover E, Huang Y, Xu L, Newcomb M, Zhang R (2010) Photocatalytic aerobic oxidation by a bis-porphyrin-ruthenium (IV) mu-oxo dimer: Observation of a putative porphyrin-ruthenium (V)-oxo intermediate. Org Lett 12(10): 2246-2249.
28. Guo M, Corona T, Ray K, Nam W (2019) Heme and nonheme high-valent iron and manganese oxo cores in biological and abiological oxidation reactions. ACS Cent Sci 5(1): 13-28.
29. Groves JT, Kruper WJ, Haushalter RC (1980) Hydrocarbon oxidations with oxometalloporphinates. Isolation and reactions of a (Porphinato) manganese(V) complex. J Am Chem Soc 102(20): 6375-6377.
30. Hill CL, Schardt BC (1980) Alkane activation and functionalization under mild conditions by a homogeneous manganese (III)porphyrin-iodosylbenzene oxidizing system. J Am Chem Soc 102(20): 6374-6375.
31. Groves JT, Lee J, Marla SS (1997) Detection and characterization of an oxomanganese (V) porphyrin complex by rapid-mixing stopped-flow spectrophotometry. J Am Chem Soc 119(27): 6269-6273.

32. Nam W, Kim I, Lim MH, Choi HJ, Lee JS, et al. (2002) Isolation of an oxomanganese(V) porphyrin intermediate in the reaction of a manganese (III) porphyrin complex and H_2O_2 in aqueous solution. Chem Eur J 8(9): 2067-2071.

33. Zhang R, Horner JH, Newcomb M (2005) Laser flash photolysis generation and kinetic studies of porphyrin-manganese-oxo intermediates. Rate constants for oxidations effected by porphyrin-Mn(V)-oxo species and apparent disproportionation equilibrium constants for porphyrin-Mn (IV)-oxo species. J Am Chem Soc 127(18): 6573-6582.

34. Jin N, Ibrahim M, Spiro TG, Groves JT (2007) Trans-dioxo manganese(V) porphyrins. J Am Chem Soc 129(41): 12416-12417.

35. Groves JT, Stern MK (1988) Synthesis, characterization and reactivity of oxomanganese (IV) porphyrin complexes. J Am Chem Soc 110(26): 8628-8638.

36. Czernuszewicz RS, Su YO, Stern MK, Macor KA, Kim D, et al. (1988) Oxomanganese (IV) porphyrins identified by resonance raman and infrared spectroscopy. Weak bonds and the stability of the half-filled t2g subshell. J Am Chem Soc 110(13): 4158-4165.

37. Fukuzumi S, Fujioka N, Kotani H, Ohkubo K, Lee YM, et al. (2009) Mechanistic insights into hydride-transfer and electron-transfer reactions by a manganese (IV)-oxo porphyrin complex. Am Chem Soc 131(47): 17127-17134.

38. Guo M, Seo MS, Lee YM, Fukuzumi S, Nam W (2019) Highly reactive manganese (IV)-oxo porphyrins showing temperature-dependent reversed electronic effect in C-H bond activation reactions. J Am Chem Soc 141(31): 12187-12191.

39. Klaine S, Bratcher F, Winchester CM, Zhang R (2020) Formation and kinetic studies of manganese (IV)-oxo porphyrins: Oxygen atom transfer mechanism of sulfide oxidations. J Inorg Biochem 204: 110986.

40. Kwong KW, Winchester CM, Zhang R (2016) Photochemical generation of manganese (IV)-oxo porphyrins by visible light photolysis of dimanganese (III) μ-oxo bis-porphyrins. Inorg Chim Acta 451: 202-206.

41. Peterson MW, Rivers DS, Richman RM (1985) Mechanistic considerations in the photodisproportionation of .mu. -oxo-bis((tetraphenylporphinato)iron (III)). J Am Chem Soc 107(10): 2907-2915.

42. Golubkov G, Bendix J, Gray HB, Mahammed A, Goldberg I, et al. (2001) High-valent manganese corroles and the first perhalogenated metallocorrole catalyst. Angew Chem Int Ed Engl 40(11): 2132-2134.

43. Zhang R, Harischandra DN, Newcomb M (2005) Laser flash photolysis generation and kinetic studies of corrole-manganese (V)-oxo intermediates. Chem Eur J 11(19): 5713-5720.

44. Kumar A, Goldberg I, Botoshansky M, Buchman Y, Gross Z (2010) Oxygen atom transfer reactions from isolated (Oxo)manganese (V) corroles to sulfides. J Am Chem Soc 132(43): 15233-15245.

45. Kwong KW, Lee NF, Ranburg D, Malone J, Zhang R (2016) Visible light-induced formation of corrole-manganese (V)-oxo complexes: Observation of multiple oxidation pathways. J Inorg Biochem 163: 39-44.

46. Lee NF, Malone J, Jeddi H, Kwong KW, Zhang R (2017) Visible-light photolysis of corrole-manganese (IV) nitrites to generate corrole-manganese (V)-oxo complexes. Inorg Chem Commun 82: 27-30.

47. Liu HY, Lai TS, Yeung LL, Chang CK (2003) First synthesis of perfluorinated corrole and its mn=o complex. Org Lett 5(5): 617-620.

48. Leznoff CC, Lever AB (1996) Phthalocyanines: properties and applications. VCH: Weinheim, Germany.

49. Sorokin AB, Kudrik EV (2011) Phthalocyanine metal complexes: Versatile catalysts for selective oxidation and bleaching. Catal Today 159(1): 37-46.

50. Sorokin AB (2013) Phthalocyanine metal complexes in catalysis. Chem Rev 113(10): 8152-8191.

51. Sorokin AB (2019) Recent progress on exploring μ-oxo bridged binuclear porphyrinoid complexes in catalysis and material science. Coor Chem Rev 389: 141-160.

52. Skipworth T, Kalaine S, Zhang R (2023) Photochemical generation and reactivity of a new phthalocyanine-manganese-oxo intermediate. Chem Commun 59(43): 6540-6543.

53. Afanasiev P, Kudrik EV, Albrieux F, Briois V, Koifman OI, et al. (2012) Generation and characterization of high-valent iron oxo phthalocyanines. Chem Commun 48(49): 6088-6090.

54. Fujii H (2002) Electronic structure and reactivity of high-valent oxo iron porphyrins. Coord Chem Rev 226(1-2): 51-60.

55. Nam W (2007) Dioxygen activation by metalloenzymes and models. Acc Chem Res 40(7): 465.

56. Sono M, Roach MP, Coulter ED, Dawson JH (1996) Heme-containing oxygenases. Chem Rev 96(7): 2841-2887.

57. Chen TH, Asiri N, Kwong KW, Malone J, Zhang R (2015) Ligand control in the photochemical generation of high-valent porphyrin-iron–oxo derivatives. Chem Commun 51(49): 9949-9952.

58. Kwong KW, Patel D, Malone J, Lee NF, Kash B, et al. (2017) An investigation of ligand effects on the visible light-induced formation of porphyrin–iron(iv)-oxo intermediates. New J Chem 41(23): 14334-14341.

59. Pan Z, Newcomb M (2011) Acid-catalyzed disproportionation of oxoiron (IV) porphyrins to give oxoiron (IV) porphyrin radical cations. Inorg Chem Commun 14(6): 968-970.

60. Ohtake H, Higuchi T, Hirobe M (1995) The highly efficient oxidation of olefins, alcohols, sulfides and alkanes with heteroaromatic N-oxides catalyzed by ruthenium porphyrins. Heterocycles 40(2): 867-903.

61. Groves JT, Bonchio M, Carofiglio T, Shalyaev K (1996) Rapid catalytic oxygenation of hydrocarbons by ruthenium pentafluorophenylporphyrin complexes: Evidence for the involvement of a Ru (III) intermediate. J Am Chem Soc 118(37): 8961-8962.

62. Zhang R, Yu WY, Wong KY, Che CM (2001) Highly efficient asymmetric epoxidation of alkenes with a D4-symmetric chiral dichlororuthenium (IV) porphyrin catalyst. J Org Chem 66(24): 8145-8153.

63. Ogliaro F, Visser SP, Groves JT, Shaik S (2001) Chameleon states: High-valent metal-oxo species of cytochrome p450 and its ruthenium analogue. Angew Chem Int Ed Engl 40(15): 2874-2878.

64. Shing KP, Cao B, Liu Y, Lee HK, Li MD, et al. (2018) Arylruthenium (III) porphyrin-catalyzed C-H oxidation and epoxidation at room temperature and [Ru^{V} (Por)(O)(Ph)] intermediate by spectroscopic analysis and density functional theory calculations. J Am Chem Soc 140(22): 7032-7042.

65. Zhang R, Vanover E, Luo WL, Newcomb M (2014) Photochemical generation and kinetic studies of a putative porphyrin-ruthenium (v)-oxo species. Dalton Transactions 43(23): 8749-8756.

66. Collman JP, Barnes CE, Brothers PJ, Collins TJ, Ozawa T, et al. (1984) Oxidation of ruthenium (II) and ruthenium (III) porphyrins. Crystal structures of μ-oxo-bis[(p-methylphenoxo) (meso-tetraphenylporphyrinato)-ruthenium (IV)] and ethoxo(meso-tetraphenylporphyrinato)-(ethanol) ruthenium (III)-Bisethanol. J Am Chem Soc 106(18): 5151-5163.

67. Rosenthal J, Luckett TD, Hodgkiss JM, Nocera DG (2006) Photocatalytic oxidation of hydrocarbons by a bis-iron (III)-mu-oxo Pacman porphyrin using O_2 and visible light. J Am Chem Soc 128(20): 6546-6547.

68. Groves JT, Quinn R (1984) Models of oxidized heme proteins. Preparation and characterization of a trans-dioxoruthe nium (VI) porphyrin complex. Inorg Chem 23(24): 3844-3846.

69. Groves JT, Quinn R (1985) Aerobic epoxidation of olefins with ruthenium porphyrin catalysts. J Am Chem Soc 107(20): 5790-5792.

70. Leung WH, Che CM (1989) High-valent ruthenium (IV) and -(VI) oxo complexes of octaethylporphyrin. Synthesis, spectroscopy and reactivities. J Am Chem Soc 111(24): 8812-8818.

71. Gross Z, Barzilay CM (1995) A novel facile synthesis of dihalogenoruthenium (IV) porphyrins. Chem Commun (12): 1287-1288.

72. Huang Y, Vanover E, Zhang R (2010) A facile photosynthesis of trans-dioxoruthenium (vi) porphyrins. Chem Commun 46(21): 3776-3778.

73. Zhang R, Huang Y, Abebrese C, Thompson H, Vanover E, et al. (2011) Generation of trans-dioxoruthenium (VI) porphyrins: A photochemical approach. Inorg Chim Acta 376(1): 152-157.

74. Abebrese C, Huang Y, Pan A, Yuan Z, Zhang R (2011) Kinetic studies of oxygen atom transfer reactions from trans-dioxoruthenium (VI) porphyrins to sulfides. J Inorg Biochem 105(12): 1555-1561.

75. Muzart J (1992) Chromium-catalyzed oxidations in organic synthesis. Chem Rev 92(1): 113-140.

76. Groves JT, Haushalter RC (1981) E.S.R. evidence for chromium (V) porphyrinates. Chem Commun (22): 1165-1166.

77. Creager SE, Murray RW (1985) Electrochemical studies of oxo(meso-tetraphenylporphinato) chromium (IV). Direct evidence for epoxidation of olefins by an electrochemically generated formal Chromium(V) state. Inorg Chem 24(23): 3824-3828.

78. Skipworth T, Khashimov M, Ojo I, Zhang R (2022) Kinetics of chromium(V)-oxo and chromium (IV)-oxo porphyrins: Reactivity and mechanism for sulfoxidation reactions. J Inorg Biochem 237: 112006.

79. Fujii H, Yoshimura T, Kamada H (1997) ESR studies of oxochromium (V) porphyrin complexes: Electronic structure of the Cr^{V}=O moiety. Inorg Chem 36(6): 1122-1127.

80. McGarrigle EM, Gilheany DG (2005) Chromium- and manganese-salen promoted epoxidation of alkenes. Chem Rev 105(5): 1563-1602.

81. Samsel EG, Srinivasan K, Kochi JK (1985) Mechanism of the chromium-catalyzed epoxidation of olefins. Role of oxochromium (V) cations. J Am Chem Soc 107(25): 7606-7617.

82. Klaine S, Lee NF, Dames A, Zhang R (2020) Visible light generation of chromium (V)-oxo salen complexes and mechanistic insights into catalytic sulfide oxidation. Inorg Chim Acta 509: 119681.

83. Lee NF, Patel D, Liu H, Zhang R (2018) Insights from kinetic studies of photo-generated compound II models: Reactivity toward aryl sulfides. J Inorg Biochem 183: 56-65.

84. Hennig H (1999) Homogeneous photo catalysis by transition metal complexes. Coord Chem Rev 182(1): 101-123.

85. Nocera DG (2012) The artificial leaf. Acc Chem Res 45(5): 767-776.

86. Nocera DG (2017) Solar fuels and solar chemicals industry. Acc Chem Res 50(3): 616-619.

87. Zhang R, Vanover E, Chen TH, Thompson H (2013) Visible light-driven aerobic oxidation catalyzed by a diiron (IV) μ-oxo biscorrole complex. Appl Catal A 465: 95-100.

88. Malone J, Klaine S, Alcantar C, Bratcher F, Zhang R (2021) Synthesis of a light-harvesting ruthenium porphyrin complex substituted with BODIPY units. Implications for visible light-promoted catalytic oxidations. New J Chem 45(11): 4977-4985.

